Fungal Ecology 61 (2023) 101199

Contents lists available at ScienceDirect

Fungal Ecology

journal homepage: www.elsevier.com/locate/funeco

Metabolic activities and ultrastructure imaging at late-stage of wood decomposition in interactive brown rot - white rot fungal combinations

Tuulia Mali [a], Karoliina Laine [a], Leena Hamberg [b], Taina Lundell [a,*]

[a] Department of Microbiology, Faculty of Agriculture and Forestry, University of Helsinki, Finland
[b] Natural Resources Institute Finland (Luke), Bioeconomy and Environment, Finland

ARTICLE INFO

Corresponding Editor: Yu Fukasawa

Keywords:
Basidiomycota
Interspecific interactions
Iron reduction
Oxalic acid
Enzyme activity
Laccase
Manganese peroxidase
Wood biodegradation
White rot
Brown rot

ABSTRACT

Basidiomycota brown rot fungus (*Fomitopsis pinicola*) and two white rot fungi (*Phlebia radiata*, *Trichaptum abietinum*) were cultivated on thin slices of spruce wood individually and in interspecies combinations. Within 12 months, *F. pinicola* substantially decomposed spruce wood observed as mass loss, also in three-species combinations. However, white rot fungi through hyphal interactions negatively affected the brown-rot indicative iron reduction capacity of *F. pinicola*. Decay-signature gene expression in mycelial interaction zones indicated suppression of brown rot mechanism but stimulation of enzymatic white-rot lignin attack by *P. radiata*. Wood ultrastructure imaging showed white-rot dominance in the fungal combinations, whereas destructive brown-rot was evident with *F. pinicola* alone. Our results confirm the dynamic pattern of enzyme production in fungal combinations, and transition from brown to white rot decomposition metabolism during the late stage of wood decay after one year of interspecific interactions.

1. Introduction

Fungi and their interspecific interactions have an important role in terrestrial ecosystems. Fungal mycelia interact with their environment by sensing and responding to the stimuli (Aleklett and Boddy 2021). Mycelial interactions and fungal communities are under transition as wood decay proceeds (Ovaskainen et al. 2013; Ottosson et al. 2014; Rajala et al. 2015). In naturally decomposing Norway spruce deadwood at a boreal forest site, a higher number of brown rot fungal species have been detected during stages of early decay and wood inhabitation, whereas white rot fungal species dominated in the later stages of decay (Rajala et al. 2015). Another study revealed that white rot species appeared both at early and late decay stages, gradually taking over as wood decomposition proceeded before ectomycorrhizal fungi finally invaded the habitat (Rajala et al. 2011).

These studies, among others, indicate that interactions in the fungal community are intricate dynamic processes. Under controlled laboratory conditions with incubation of fungi on solid wood, composition of the fungal community influences secreted enzyme production, emission of volatile organic compounds (VOC), and the rate and specificity of decomposition of wood lignocellulose components (Hiscox et al. 2010; El Ariebi et al. 2016; Mali et al. 2017, 2019). Dynamic mycelial encounters in the fungal communities may increase the rate of wood decomposition (Mali et al. 2017).

Wood as substrate and living environment is a demanding habitat for microbes (Baldrian 2017). Anatomically, fully lignified coniferous xylem (softwood) like Norway spruce wood is mainly composed of long, hollow, and thick-walled tracheids arranged into earlywood and latewood sections (Sjöström 1993). The compact plant cell walls in xylem tracheids are multi-layered (middle lamella, primary cell wall, secondary cell walls S1–S3), and the layers are different in ultrastructure and chemical composition (Eriksson et al. 1990; Sjöström 1993). The outermost middle lamellae attach the long tracheids together and contain pectin and lignin. The thick secondary cell walls are lignified and contain most of the cellulose microfibrils and the biomass of the wood cell-wall lignocellulose (Eriksson et al. 1990).

Decomposition of deadwood is an ability restricted predominantly to the fungal phylum *Basidiomycota* class *Agaricomycetes*, which includes white rot, brown rot, soft rot, litter-decomposing, and ectomycorrhizal species of fungi (Floudas et al. 2012; Lundell et al. 2014; Riley et al.

* Corresponding author. Department of Microbiology, University of Helsinki, Biocenter 1, P.O.Box 56, FI-00140, Finland.
E-mail address: taina.lundell@helsinki.fi (T. Lundell).
URL: https://researchportal.helsinki.fi/en/persons/taina-lundell (T. Lundell).

https://doi.org/10.1016/j.funeco.2022.101199
Received 17 February 2022; Received in revised form 7 September 2022; Accepted 11 September 2022
Available online 30 September 2022

2014; Nagy et al. 2016). Moreover, white rot and brown rot fungal species have their specific traits of decomposing and modifying the wood cell-wall lignocellulose components (cellulose, hemicellulose, pectin, and lignin) to access carbohydrates as nutrients for growth (Lundell et al. 2014; Rytioja et al. 2014).

White rot fungi secrete carbohydrate active enzymes (CAZymes, Lombard et al., 2014) and oxidoreductases to decompose and modify all wood components (Floudas et al. 2012; Yakovlev et al. 2013; Lundell et al. 2014; Riley et al. 2014; Rytioja et al. 2014). Brown rot fungi are considered to break down cellulose and hemicellulose primarily non-enzymatically by secretion of oxalic acid and generation of radical oxygen species (ROS) via Fenton chemistry followed by secretion of hydrolytic enzymes (Xu and Goodell 2001; Eastwood et al. 2011; Arantes et al. 2012; Zhang et al. 2016; Presley and Schilling 2017).

Previously, we found patterns of changes in fungal mycelial growth and enzyme activities in combination cultivations of the brown rot species *Fomitopsis pinicola* together with several species of white rot fungi (Mali et al. 2017). Temporal changes of fungal interaction biochemistry were followed during the early stage of wood decay on spruce wood sawdust. Together with enzyme activity profiles, signature characteristics of emission of VOCs (mainly wood terpenoids) of brown rot or white rot in decomposition of spruce were observed (Mali et al. 2019).

In this study, we continued the previous experimental setups of fungal combinations on thin vertical slices of spruce wood for a longer period focusing on both the biological and wood anatomical changes at the late stage of fungal decay (in an experiment of 1-y duration). We monitored the three fungi both separately and in interactive combinations, and assessed their metabolism and mechanisms of wood decomposition in the hyphal interaction zones. Hypotheses of this study were the following: presence of competing species affect hyphal response and wood decay activities in each fungus; and decomposition of wood is influenced both by the fungal species combination and duration of hyphal interactions. Our results show that metabolic activities in the hyphal interaction zones include both white rot enzymatic and brown rot oxidative chemistry. However, the brown rot decay is suppressed by the white rot species activity. Moreover, the switch to white rot mechanism was evidenced by noticeable expression of genes specific to enzymatic lignin-attack and changes in the wood ultrastructure.

2. Materials and methods

2.1. Fungal isolates and culture conditions

Fungal isolates of the order *Polyporales* (phylum *Basidiomycota*, class *Agaricomycetes*) species *Fomitopsis pinicola* (Fp, FBCC1181) and *Phlebia radiata* (Pr, FBCC0043), and *Trichaptum abietinum* (Ta, FBCC0110) of the order *Hymenochaetales* were stored at the University of Helsinki Microbial Domain Biological Resource Center HAMBI FBCC fungal culture sub-collection (https://www.helsinki.fi/en/infrastructures/biodiversity-collections/infrastructures/microbial-domain-biological-resource-centre-hambi). Fungal isolates were phylogenetically confirmed by ITS-sequence analysis in a previous study (Mali et al., 2017) accessions [LT844580, LT844581, LT844582]. The fungi were cultivated on 2% malt extract agar (MEA, pH 5.5) at 25 °C in the dark for 1 week before initiation of cultivation on Norway spruce (*Picea abies*) wood veneer slices (2.5 cm width × 6 cm length × 0.5 cm thickness; obtained from LUT University, Finland).

2.2. Co-cultivation of fungi on spruce veneer slices

Fungal isolates were cultivated as single-species or two or three-species combinations on spruce veneer slices. Dry veneer slices were autoclaved (121 °C, 15 min). Three of the slices were placed in a large (13-cm diameter) sterile plastic Petri dish as mounted on water agar (1.5% agar in deionized water, autoclaved prior to use) to maintain 60% moisture content during incubation. For enzyme assays, RNA extraction, and organic acid analyses, six veneer slices were inoculated for each set-up of fungal combinations as well as for individual species and controls without any fungus (Fig. 1). In three-species combinations, the brown rot species *F. pinicola* (Fp) was always placed in the middle (Fig. 1C). In addition, for scanning electron microscopy (SEM) and transmission electron microscopy (TEM) imaging, additional spruce veneer cultivations were set.

The veneer cultivations were incubated in the dark at room temperature (20–23 °C) for 12 months to investigate the outcome of long-term fungal interactions at later stage of wood decay. Moisture content in the veneer slices was maintained during the cultivations by regularly adding sterile ultrapure water onto the bottom agar. After incubation, the cultivated veneer slices were frozen with liquid nitrogen and stored at −80 °C sealed in aluminium foil for further analyses (see below). The fungal interaction zones and mycelial fronts were determined visually on each veneer slice prior to cutting off the respective regions (Fig. 1D–F).

2.3. Real-time qRT-PCR of enzyme-encoding genes

Total RNA was extracted from the cut thin pieces of the frozen spruce wood veneer cultures. Wood pieces were snap-frozen in liquid nitrogen and ground to powder with a mortar and pestle. All equipment were acid-washed and heat sterilized or treated with RNaseZap (Thermo Fisher) before use. RNA was purified from ground wood samples with EZ-10 Total RNA Mini-Preps kit (Bio Basic Inc.) according to the manufacturer's instructions. Concentration and purity of nucleic acids were analysed with NanoDrop One Microvolume UV Spectrophotometer (Thermo Fisher Scientific). cDNA was synthesized from 100 to 250 ng of total RNA using Maxima First Strand cDNA Synthesis Kit with dsDNase (Thermo Fisher Scientific) according to the manufacturer's instructions.

To analyse expression of brown-rot indicative enzymes and proteins, RNA-Seq transcriptome data of *F. pinicola* FBCC1181 (unpublished data) were used to search genes upregulated on spruce wood substrate for real-time quantitative reverse transcription PCR (real-time qRT-PCR). Gene-specific primers were designed for Fp (Table 1) and qRT-PCR analysis was performed according to Mäkinen et al. (2018). The four sets of qPCR primers had excellent amplification efficiency (90–102%, Table 1). To investigate whether undesirable amplification occurred, primers designed specifically for transcripts of Fp genes were qPCR tested against the cDNA of RNA extracted from single-species cultures of *T. abietinum* (Ta) and *P. radiata* (Pr). Primers specific to Pr gene transcripts were designed as previously described (Table 1, Hildén et al. 2005; Mäkinen et al. 2018) and tested against the cDNA of RNA extracted from Fp and Ta single-species cultures. Selected genes of induced white-rot type of wood decay were targeted in the qRT-PCR analysis. These enzyme-encoding genes were previously shown to be upregulated in Pr during the early phase of hyphal inhabitation and decomposition of spruce wood (Kuuskeri et al. 2016) as well as on wood-based waste lignocellulose (Mäkinen et al. 2018; Mattila et al. 2020).

For analysis, Framestar 96-well semi-skirted, frosted-well PCR plates (4titude ltd.) were applied in an Applied Biosystems QuantStudio 3 Real-Time PCR system. The 12.5-µl reaction mixtures contained Maxima SYBR Green qPCR Master Mix (Thermo Fisher Scientific) with 3 µM of each primer and 2.5 µl of the diluted cDNA template. RT-qPCR was performed, and amplification efficiency and relative fold change of gene expression were calculated according to a previous study (Mäkinen et al. 2018). In the amplifications, specific amplicon primers for two reference gene (*sar* and *ubc*) transcripts were applied for both Fp and Pr (Table 1). Use of transcript amplicons of more than one reference gene in real-time RT-qPCR analysis has been noticed to improve reliability and accuracy in calculation of relative expression of differentially regulated genes under varying cultivation conditions in filamentous fungi of Ascomycota and Basidiomycota (Steiger et al. 2010; Castanera et al. 2015; Llanos

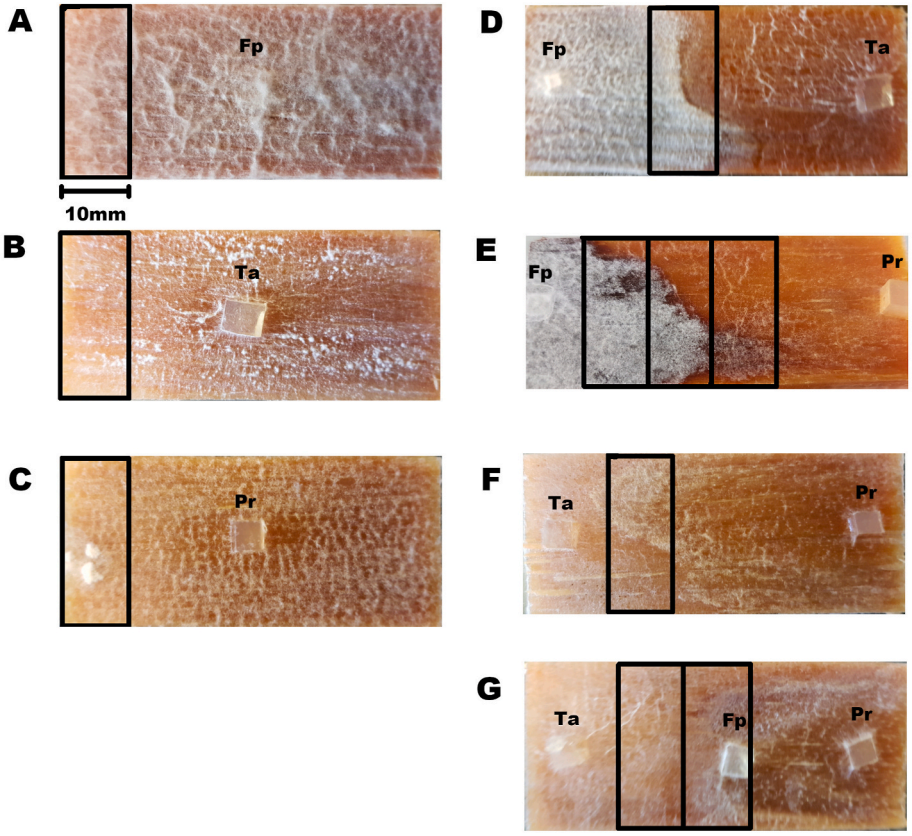

Fig. 1. Digipictures of mycelial growth on the spruce wood veneer slices after 1 y of incubation. Pre-cultivated 5 mm × 5 mm agar plugs were initially placed on the top of each slice (A–C) the single fungal species (Fp, *Fomitopsis pinicola*, brown rot fungus; Ta, *Trichaptum abietinum*, white rot fungus; Pr, *Phlebia radiata*, white rot fungus) cultivation, (D–F) combination of two species per veneer slice, or (G) the three fungi combined on the same spruce wood veneer slice. For further analyses, 10 mm wide sections from (A–C) one end of the veneer slice were cut in the case of single fungal species; or (D–F) from the interaction zone and (E) next to that zone on both sides in the case of combination of *F. pinicola* and *P. radiata*; or (G) from the corresponding interspecific interaction zones in case of all three fungi on the same veneer slice. For all single-species and combination cultures, six spruce veneer slices were cultivated (n = 6 for biological replicates). Examples of one image of the six replicates are shown.

et al. 2015) thus resulting in improved relevancy in interpretation of differences in gene expression, as was noticed in our previous study using three reference genes (*sar*, *ubc* and *fis*) (Mäkinen et al. 2018). Due to the low amount of retrieved RNA or strong down-regulation of the genes on some veneer slice samples, no detection of one or both of the reference genes or tested genes after >35 cycles of amplification was observed in some combinations. Therefore, results are not available for every slice. These cases are indicated in the figure legends.

2.4. Extraction and analyses of secreted proteins and oxalic acid

To determine the fungal activities of Fp (*F. pinicola*), Pr (*P. radiata*), and Ta (*T. abietinum*) in the mycelial interaction zones and their vicinity on the cultivated veneers (Fig. 1D–F), extracellular proteins and oxalic acid were extracted from cut sections of three similar veneer slice cultivations. Approximately 2.5 cm × 1 cm pieces were cut off from the veneers. Extracellular proteins and oxalic acid (as free non-chelated acid in the water phase) were extracted at +4 °C with 25 mM sodium acetate buffer, pH 5.5, including 0.2 mM phenylmethane-sulphonyl fluoride as inhibitor for protease activity (Mäkelä et al. 2002; Kuuskeri et al. 2016; Mali et al. 2019). Bound oxalate was dissolved and extracted with 1.5 M HCl. Protein and acid extracts were stored at −20 °C until further analysis. Protein was quantitated with the 96-well plate microassay method using Bradford reagent according to the manufacturer's instructions (Bio-Rad). Concentration of fungal-produced oxalic acid (as free acid in the water phase and in extracts of bound oxalate) in the samples was analysed by applying the previously optimized HPLC method, with detection limit of 10 μM (Mattila et al. 2017).

2.5. Enzyme activity and iron reduction assays

Laccase and MnP activities were determined according to previously adopted methods (Wariishi et al. 1992; Slomczynski et al. 1995; Hildén et al. 2005; Rytioja et al. 2014; Kuuskeri et al. 2015) to monitor production of extracellular oxidoreductases by the white-rot fungi Pr and Ta. Lignin peroxidase (LiP) assay using veratryl alcohol as substrate was not successful probably due to interfering compounds dissolved from spruce wood, which was likewise noticed before in a similar study (Kuuskeri et al. 2015). For laccase activity, ABTS (2,2′-azino-bis(3 ethylbenzothiazoline-6-sulphonic acid), and for MnP activity, Mn^{2+} ions were used as the respective substrates in 10 mM sodium malonate buffer set to pH 3.0. Activity assays were also performed in malonate buffer pH 4.5. However, the reaction rates obtained with pH 3.0 or pH 4.5 were almost similar. To detect brown rot decay activity of Fp and promotion of Fenton chemistry, iron-reduction activity as reduction of Fe^{3+} to Fe^{2+} was analysed using a previously modified and adopted method (Shah et al. 2015, 2018).

2.6. Wood mass loss and Klason lignin analysis

Pieces of the veneers were dried for 72 h at 90 °C for analysis of wood-mass loss as change in dry weight of the spruce veneer cultivations of Fp, Pr, and Ta. The initial dry weight of the spruce veneer slices was measured prior to inoculation. For analysis of Klason lignin and acid-soluble lignin, two separate samples from each of the three individual spruce veneer cultivations were made by cutting the specific pieces from individual cultivations of Fp and Pr (Fig. 1A,D) and their two-species combination (FpPr) (Fig. 1B,E) and dried for 72 h at 90 °C. Non-inoculated spruce veneer control slices incubated for 12 months under the same conditions were likewise selected for sample preparation. Dried pieces of wood were ground with a mortar and pestle and sieved (1-mm particle size metal screen). Klason lignin and acid-soluble lignin content were measured and calculated according to previously adopted methods (Browning 1967; Hatfield and Fukushima 2004; Kuuskeri et al. 2016).

Table 1
Primers designed for this study for real-time qRT-PCR analysis of protein-coding gene transcripts of *F. pinicola* FBCC1181 (Fp) and those designed earlier for *P. radiata* FBCC0043 (Pr). Protein ID refers to homologs searched in the genomic data of *F. pinicola* isolate FP-58527 SS1 (v3.0) available at the JGI MycoCosm (https://mycocosm.jgi.doe.gov/Fompi3/Fompi3.home.html). GeneIDs for annotated *P. radiata* genes are reported in previous studies (Kuuskeri et al., 2016; Mäkinen et al., 2019).

Gene	Protein function	Protein ID or GeneID	Primers in qRT-PCR	Sequence 5′-3′	Product length (bp)	Amplification efficiency (%)	Reference for primers
Fp mco1	Multicopper oxidase, laccase	281599, Fpmco1	Fp_mco1_f	ACTTCACATTTGACAACTGGAC	162	102	This study
			Fp_mco1_r	CGTGGTACAAATCCGAGAC			
Fp fr1	Ferric reductase	1026244	Fp_fr_f1	TGAACATTGGTAGCTCGTACAC	102	97.8	This study
			Fp_fr_r1	GGTCAGTGGTGTTGATAAATTCC			
Fp sar1	Small GTP-binding protein SAR1	159569	Fp_sar_f	CCTTCACCCTACATCCGAG	99	97.3	This study
			Fp_sar_r	TAGTCACGCCAAAGTCGG			
Fp ubc6	Ubiquitin-conjugating enzyme	19405	Fp_ubc_f1	ATCCAGGAACGTGGAACC	109	90	This study
			Fp_ubc_r1	TTGTCGGTGGATGTGACTG			
Pr lip2	Lignin peroxidase	Minus.g6827	Lip2F1	GACCATTTGTTGGCTCGTGAC	106	96.1	Mäkinen et al. (2018)
			Lip2R1	CCCATAGCACCGAAGATAAACTG			
Pr mnp2	Manganese peroxidase	Plus.g10562	PrMnP2FqPCR	GTTCCCCACGCTGTCCAC	133	90.1	Mäkinen et al. (2018)
			MnP2rev	CTACGAGTCGTCTGCACCAC			Hildén et al. (2005)
Pr lpmo1	Lytic polysaccharide monooxygenase	Plus.g9320	LPMO_AA9.1F2	GCTGAAGTCATTGCTCTCCAC	171	98.4	Mäkinen et al. (2018)
			LPMO_AA9.1R2	ACGACTGGTAAATGTTGATGAGG			
Pr eg1	β-1,4-endoglucanase	Plus.g7451	EG_GH5.3F1	CGTGCTTACTACCCTCGTG	108	96.1	Mäkinen et al. (2018)
			EG_GH5.3R1	GGAGTTCAAGAATTGTTCGCAG			
Pr xyn1	β-1,4-endoxylanase	Plus.g3697	XYN_GH11.1F1	TCATCCGGCACAGTTGCT	112	96.3	Mäkinen et al. (2018)
			XYN_GH11.1R1	CATTGGCAGTAGTAGGTGTTGG			
Pr bgl1	β-glucosidase	Minus.g7505	BGL_GH3.1F1	ACCACTGTAACTACATCGCTC	113	97.6	Mäkinen et al. (2018)
			BGL_GH3.1R1	GATATAACCCTCACCGCTATCTG			
Pr sar1	GTP-binding protein	Plus.g4563	Sar1F1	GACATTTGCAAGCTCGTCGG	181	92.6	Mäkinen et al. (2018)
			Sar1R1	TGCGTCGATCTTGTTACCGAG			
Pr ubc6	Ubiquitin conjugating enzyme	Minus.g11916	Ubc6F1	CACAAGCGACTGACCAAGGA	158	91.6	Mäkinen et al. (2018)
			Ubc6R1	CATTAGTACGCCGTGGTACTCTC			

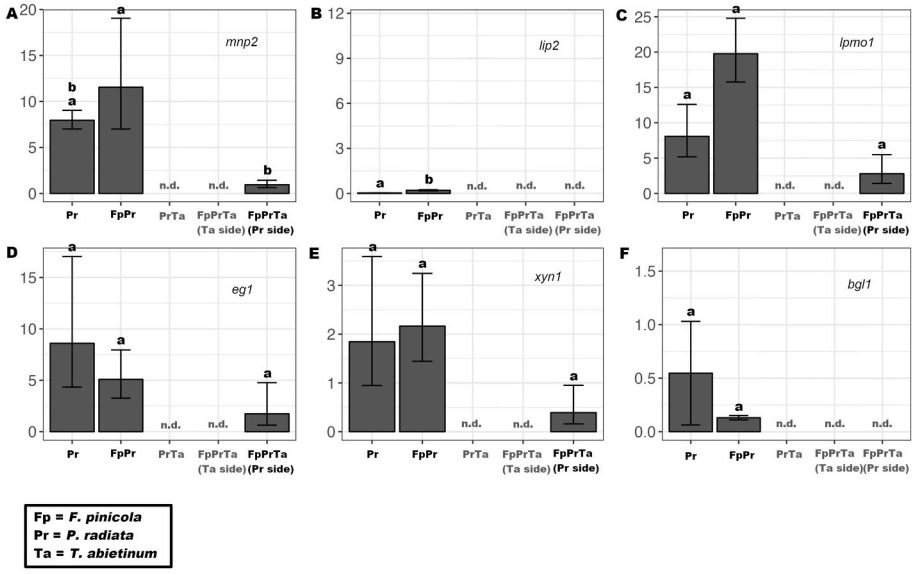

Fig. 2. Real-time qRT-PCR results of relative fold change of expression of selected white rot lignocellulose-degrading enzyme-encoding genes (A) *mnp2*, (B) *lip2*, (C) *lpmo1*, (D) *eg1*, (E) *xyn1*, and (F) *bgl1* of *P. radiata* after one-year of growth on spruce wood veneers. Transcript signals of *sar1* and *ubc6* genes were used to normalize transcript abundances. Y axis represents the relative expression level of each gene against expression of reference genes. Prediction (A, C-E) or mean average values (B, F) ($n = 3$ parallel cultures) with standard errors are presented. In (A), prediction with standard error based on linear models are presented, and the letters indicate statistically significant differences between single-species and fungal combinations (ANOVA, Tukey test $p < 0.05$). In (B), *t*-test was performed, and letters indicate statistical difference ($p < 0.05$). In (C–F), no statistically significant differences were observed. n.d. (not detected) refers to cases with target gene amplification from less than 3 parallel cultures (n = 1–2) thereby not allowing statistical testing.

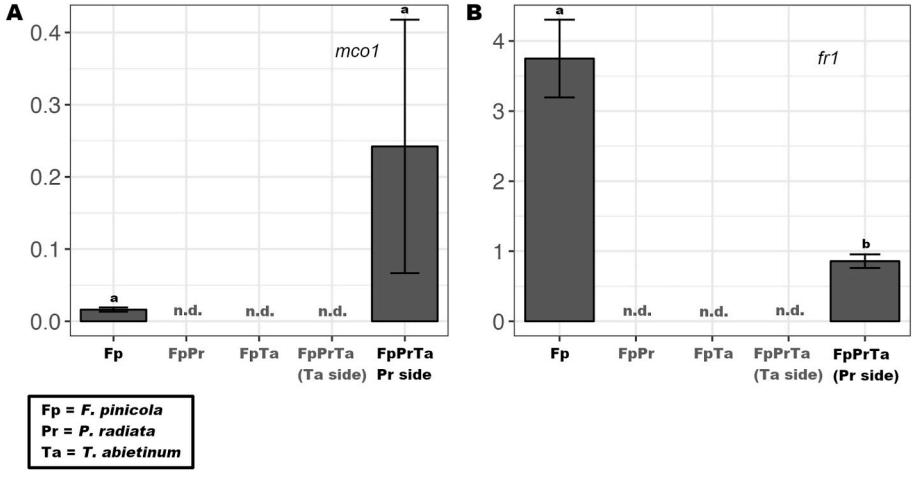

Fig. 3. Real-time qRT-PCR results of relative fold change of expression of two selected genes (A) *mco1* and (B) *fr1* of *F. pinicola* connected to brown rot decay of wood. Transcript signals were obtained after one-year of growth on spruce wood veneers. *F. pinicola sar1* and *ubc6* genes were used to normalize transcript abundances. Y axis represents the relative expression level of each gene against expression of reference genes. Mean average values ($n = 3$ parallel cultures) with standard errors are presented. In (A), no statistical difference was observed. In (B), *t*-test was performed, and letters indicate statistically significant difference. n.d. (not detected) refers to cases with target gene amplification from less than 3 parallel cultures (n = 1–2) thereby not allowing statistical testing.

2.7. Imaging of the wood veneer slices and electron microscopy

Mycelial location and interactions on the spruce wood veneer slices were photographed using Nikon D3500 digital camera after one year of incubation (Fig. 1A–C). Sections from frozen wood slices were cut for SEM (Scanning Electron Microscopy) and TEM (Transmission Electron Microscopy) analyses. Sample preparation and imaging were performed at the EMBI Electron Microscopy Unit of the University of Helsinki Institute of Life Science BioImaging infrastructure (https://www.helsinki.fi/en/infrastructures/bioimaging/embi). The decayed and intact wood sections were fixed with 2% glutaraldehyde in 0.1 M sodium phosphate buffer for 3.5 h at room temperature. After washing the samples with the 0.1 M sodium phosphate buffer overnight at +4 °C, samples were post-fixed with 2% $OsSO_4$ for 2 h and then washed with buffer at room temperature. The wood sections were dehydrated with increasing concentrations of ethanol (50–100%) and dried in an Automated Critical Point Dryer Leica EM CPD300. Samples for SEM were then coated with platinum using a Quorum Q150TS turbomolecular-pumped high resolution coater. After dehydration, the samples for TEM were incubated with acetone, and then embedded gradually into low-viscosity agar resin (50–100%) and hardened overnight at 60 °C. Ultrathin slices (≤100 nm) of wood samples were sectioned for TEM. Images were taken with a FEI Quanta 250 Field Emission Gun SEM and Jeol JEM-1400 TEM.

2.8. Statistical analyses

Differences in the relative fold change of expression of the Pr genes *mnp2*, *lpmo1*, *eg1*, and *xyn1* (n = 9) calculated from real-time qRT-PCR data; enzyme activity values (nkat *(g dw)$^{-1}$) (n = 24); and iron-reduction capacity as concentration of released Fe^{2+} ($n = 24$) between the single species and fungal combination cultures were analysed using linear models and ANOVA with subsequent Tukey test with R software (R Development Core Team, 2018). Scores were root-transformed, log-transformed, or logit-transformed when needed (Warton and Hui 2011). Differences in the relative fold change of expression of the Pr genes *lip2* and *bgl1* and Fp genes *mco1* and *fr1* were tested between slices where the fungal species were cultivated alone (either *P. radiata* Pr or *F. pinicola* Fp) and those slices where the same fungal species were cultivated together and with the third fungal species (combinations FpPr, FpPrTa). This was performed using a paired two-tailed *t*-test, since the differences were tested between two groups.

Differences in wood-mass loss, Klason lignin content, and acid-soluble lignin content between Fp and other fungal species alone (Ta or Pr), in fungal species combinations (FpTa, FpPr, PrTa, or FpPrTa), or in non-inoculated spruce veneer without fungi were estimated using linear models with Benjamini-Hochberg adjusted *p*-values. Scores were logit-transformed when needed (Warton and Hui 2011). For all analyses,

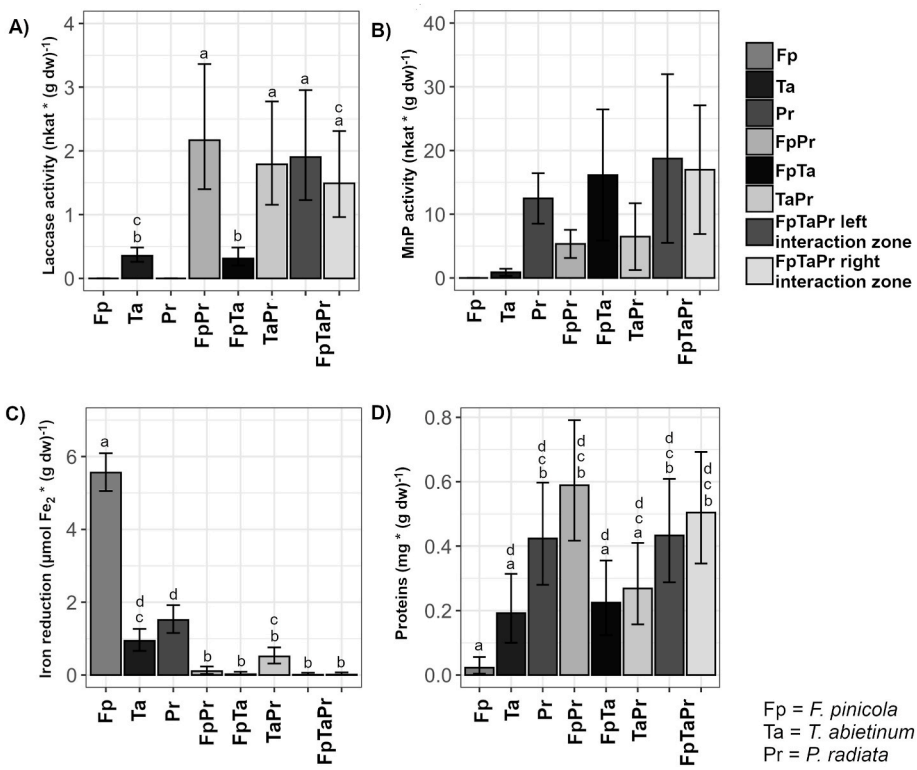

Fig. 4. Activities of (A) laccase, (B) manganese peroxidase and (C) iron reduction, and (D) estimated extracellular protein concentration on spruce wood veneers after twelve months of single fungal species or species combination cultivations (n = 18–24). From the three species combination (FpTaPr), two mycelial interaction zones were sectioned: left side of FpTa interaction, right side of FpPr interaction (Fig. 1G). Predictions with standard errors based on linear models are presented. Values were calculated in relation to total dry weight of the cultured veneer solids. In (A, C) and (D), the small letters indicate statistically significant differences between the single-species and fungal combinations (ANOVA, Tukey test $p < 0.05$).

values of the three biological replicate cultures and control samples were used. p-values < 0.05 were considered as statistically significant. For linear models and ANOVA, small letters in the figures (Figs. 2–4) indicate statistical significance. The same letters indicate similarity.

3. Results

3.1. Expression of white rot and brown rot signature genes during interactions

For analysis of fungal gene expression, sections of 10 mm width were cut from frozen wood veneer slices of single-species mycelial cultivations (Fig. 1A–C) and interacting combinations of the brown rot fungus *F. pinicola* and the white rot fungi *P. radiata* and *T. abietinum* (Fig. 1D–G) and subjected to extraction of RNA (see Materials and methods). According to real-time qRT-PCR data, all the selected six enzyme-encoding genes were expressed in *P. radiata* (Pr) mycelium growing on spruce wood for one year alone (Figs. 2A and 1C). Interestingly, interaction with the brown rot fungus *F. pinicola* (Fp) influenced upregulation of the two *P. radiata* lignin-attacking class-II peroxidase-encoding genes Pr *lip2* and Pr *mnp2* (not statistically significant) (Fig. 2A and B; FpPr interaction zone sections, example in Fig. 1E). The strongest effect of interaction with Fp was observed in the 10-fold more abundant expression of Pr *lip2*, which was expressed at low transcript quantities in the Pr mycelium alone (Fig. 2B).

A similar stimulated response of *P. radiata* gene expression was observed for the Pr *lpmo1* gene encoding a cellulose-attacking oxidoreductase, lytic polysaccharide monooxygenase (Table 1; Mäkinen et al. 2019). Expression of Pr *lpmo1* transcripts was 2-fold more abundant in the FpPr interaction zone (Fig. 1E, middle section) than in Pr mycelium alone (Fig. 1C), although the result was not statistically significant (p = 0.27) (Fig. 2C). The two cellulose-decomposing hydrolytic enzyme-encoding genes *eg1* and *bgl1* of Pr, and the xylan-degrading enzyme-encoding gene Pr *xyn1* were expressed at constant level in all combinations: no statistically significant differences were found (Fig. 2D–F).

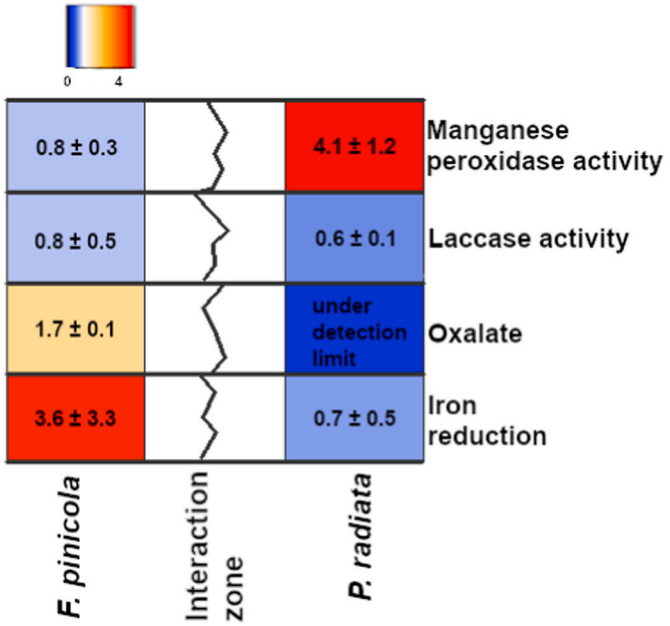

Fig. 5. Illustration of relative activities of oxidoreductase enzymes, concentration of bound oxalate, and activities of iron reduction in the different mycelial zones of the brown rot – white rot combination culture (FpPr) on the spruce wood veneer slices. Activity mean values with standard deviation were normalized relative to the values obtained in the interaction zone, which was given the value 1 in each case.

Hyphal contact with the third species *T. abietinum* (Ta), the second white rot fungus, led to a different type of regulation of gene expression. Introduction of Ta to the FpPr interaction apparently suppressed expression of the Pr *mnp2* gene during the late phase of decay (Fig. 2A; interaction zone FpPrTa, example in Fig. 1G left section). In the white

rot - white rot combination of PrTa (Fig. 1F), transcripts of the Pr genes showed relative fold-changes even below the qRT-PCR detection limit (data not shown since no detection after >35 cycles of amplification was observed in some biological replicates).

Expression of the two *F. pinicola* signature genes selected for indication of brown rot metabolism showed opposite responses to the interspecific hyphal interactions on spruce veneer slices. The Fp *mco1* gene was highly induced in the FpPr hyphal interaction zone in the three-species combination cultivation (example in Fig. 1G, right section), although the result was not statistically significant (Fig. 3A, FpPrTa (Pr side)). Fp *mco1* gene putatively encodes a multicopper oxidase (homolog 281599 in *F. pinicola* FP-58527 SS1 v3.0 genome, https://mycocosm.jgi.doe.gov/Fompi3/Fompi3.home.html). Notably, Fp *mco1* gene was expressed in very low transcript quantities by Fp mycelium alone on spruce veneers (Figs. 3A and 1A). Interestingly, and in contrast to expression of the *mco1* gene, expression of the iron-reduction involved enzyme ferric reductase-encoding gene *fr1* was strongly downregulated in the three species combination FpPrTa (Ta side, Pr side) in the presence of the white rot fungi (Fig. 3B). This contrasts with the higher level of expression detected with Fp mycelium alone growing on the spruce veneers (Fig. 3B, Fp; Fig. 1A).

3.2. Enzyme activities, iron reduction, and wood-bound oxalate

After 12 months, laccase activity was observed in the interaction zones on spruce veneers with fungal combinations including either of the white rot species *P. radiata* (Pr) or *T. abietinum* (Ta), and with Ta alone (Fig. 4A). The highest laccase activities were detected in combinations including Pr – although laccase activity was diminutive when Pr was growing as single-species on the spruce veneers. No laccase activity was detected on veneers incubated with the brown rot fungus Fp alone (Fig. 4A). In the combinations FpPr, TaPr, and FpTaPr high laccase activities were especially detected in their hyphal contact interaction zones. These observations indicate that hyphal interaction with another fungus – irrespective of white or brown rot species - stimulates laccase production in the white rot fungi, also when growing on wood as substrate.

Production of MnP activity showed a different pattern. MnP activity was observed both in the combination cultures as well as in the single-species white rot cultures (Pr or Ta) on the spruce veneer slices (Fig. 4B). As expected, the two white rot fungi Pr and Ta produced MnP in both mycelial interaction zones in the three-species combination FpPrTa. In all, no such stimulation in MnP activity was detected due to interspecies interaction as was observed with laccase production. This was further inspected in detail in the white rot – brown rot interaction zone (Fig. 5).

The highest values of iron reduction activity were observed in the single-species cases of the brown rot fungus Fp (Fig. 4C). Combination with the white rot fungi Ta and Pr, however, caused a negative effect on iron reduction activity in the mycelial interaction zones. Interestingly, the white rot fungi (Pr and Ta) alone produced some iron reduction activity but at significantly lower level than detected with the brown rot fungus Fp alone.

Regarding production of extracellular proteins by the fungal mycelia while growing on wood, the highest concentrations were detected on veneer slices including the white rot fungus Pr, also in the fungal combinations (Fig. 4D). Noticeable is the very low protein level measured for the brown rot fungus Fp, less than 1/10 of the values obtained for the combinations FpPr and FpTaPr ($p < 0.05$). These results demonstrate the high capacity of protein and enzyme secretion by mycelia of white rot fungi in comparison to the brown rot fungus Fp.

After 1 y, fungal-produced dissolved free oxalic acid was not anymore present in the spruce wood veneers. Instead, bound oxalate was detected in the single-species cases of the brown rot fungus Fp (mean ± SD = 8.7 ± 7.4 mmol/g dw) and some in the combination FpPr (Table 2). Unexpectedly, no oxalate or free oxalic acid was observed in any of the spruce wood veneers cultivated with either of the white rot fungi (Pr or Ta) in their single-species cases or in their interactive combinations (TaPr and FpTaPr) (Table 2). The same was observed for the combination FpTa.

3.3. Brown rot - white rot fungal interaction on spruce wood veneer slices

In closer view to the brown rot – white rot hyphal interaction zone of the combination FpPr on spruce wood veneers, the negative effect of

Table 2
Amount of bound oxalate in the spruce wood veneers after 12 months of fungal growth. Mean average values ($n = 3$) with standard deviation (SD) are presented. Fp, *F. pinicola*; Pr, *P. radiata*; Ta, *T. abietinum*. Coefficients (Coeff), standard errors (SE) and *p*-values (linear model) of the FpPr combination zones were compared to the veneers with Fp mycelium alone.

Fungal combination/Section of the spruce veneer	Amount of oxalate (μmol * g^{-1} total dry weight) ± SD	Coeff ± SE[a]	*p*-value[a]
Fp (intercept)	8.7 ± 7.4	1.5 ± 0.7	0.1
Pr	Udl[b]	Na[c]	Na
Ta	Udl	Na	Na
FpPr, Fp mycelium zone	1.9 ± 1.4	−1.2 ± 1.0	0.2
FpPr, middle interaction zone	1.1 ± 0.9	−1.7 ± 1.0	0.3
FpPr, Pr mycelium zone	Udl	Na	Na
FpTa	Udl	Na	Na
PrTa	Udl	Na	Na
FpPrTa, Ta side	Udl	Na	Na
FpPrTa, Pr side	Udl	Na	Na

[a] Log-transformation was used for statistical analysis.
[b] Udl = Under detection limit.
[c] Na = Not available, statistical analysis was not performed.

Table 3
Mass loss (%) of spruce wood veneer slices after 12 months of fungal growth. Mean average values ($n = 3$) with standard deviation (SD) are presented. Fp, *F. pinicola*; Ta, *T. abietinum*; Pr, *P. radiata*. Coefficients (Coeff), standard errors (SE) and Benjamini-Hochberg adjusted *p*-values (linear model) of the different fungal species present in the cultivation were compared to spruce incubation without fungi.

Species combination	Mass loss (%) ± SD	Coeff ± SE[a]	*p*-value[a]
Spruce without fungi	0.4 ± 0.1	−1.0 ± 0.2	$7.6 * 10^{-4}$
Fp	37.4 ± 4.7	4.6 ± 0.3	$2.0 * 10^{-9}$
Pr	20.0 ± 2.9	4.0 ± 0.3	$2.8 * 10^{-9}$
Ta	17.4 ± 2.1	3.9 ± 0.3	$3.8 * 10^{-9}$
FpPr	31.7 ± 9.0	4.4 ± 0.3	$2.0 * 10^{-9}$
FpTa	24.8 ± 11.2	4.1 ± 0.3	$2.6 * 10^{-9}$
PrTa	22.3 ± 1.3	4.1 ± 0.3	$2.6 * 10^{-9}$
FpPrTa	21.4 ± 0.5	4.1 ± 0.3	$2.6 * 10^{-9}$

[a] Log-transformation was used for statistical analysis.

Table 4
Klason lignin and acid-soluble lignin content in spruce wood veneer slices after 12 months of fungal growth and wood decomposition. Mean average values ($n = 3$) with standard deviation (SD) are presented. Fp, *F. pinicola*; Pr, *P. radiata*. Benjamini-Hochberg adjusted *p*-values based on results of linear models of each fungal species present were compared to spruce without fungi.

Species combination	Klason lignin (%)[a] ± SD	Acid-soluble lignin (%)[a] ± SD
Spruce without fungi	21.3 ± 0.6	0.5 ± 0.0
Fp	32.3 ± 2.7[b]	0.9 ± 0.1[b]
Pr	22.7 ± 4.1	0.8 ± 0.1[b]
FpPr	46.9 ± 3.7[b]	1.1 ± 0.1[b]

[a] Logit-transformation was used for statistical analysis.
[b] Statistically significant (adjusted *p*-value < 0.05) increase of Klason lignin content compared to spruce without fungi.

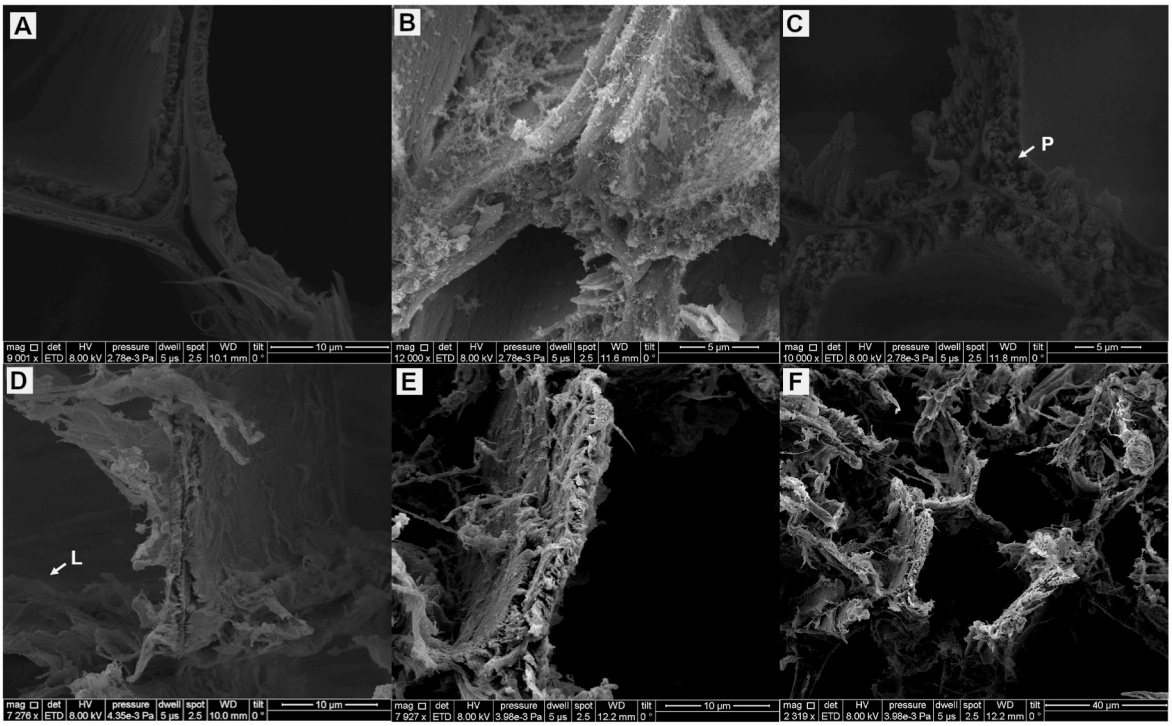

Fig. 6. SEM images of cross-sections of the spruce veneer slices after 1 y of fungal growth. (A) Non-inoculated wood; (B–C) *F. pinicola* inhabited, brown rot decayed wood; (D) *T. abietinum* colonized and degraded wood; (E–F) *P. radiata* colonized, white rot decayed wood. (P = porous and loose wood cell wall, L = layers peeled off within the wood secondary cell wall). Scale bars are 10 μm (A, D, E), 5 μm (B, C), and 40 μm (F).

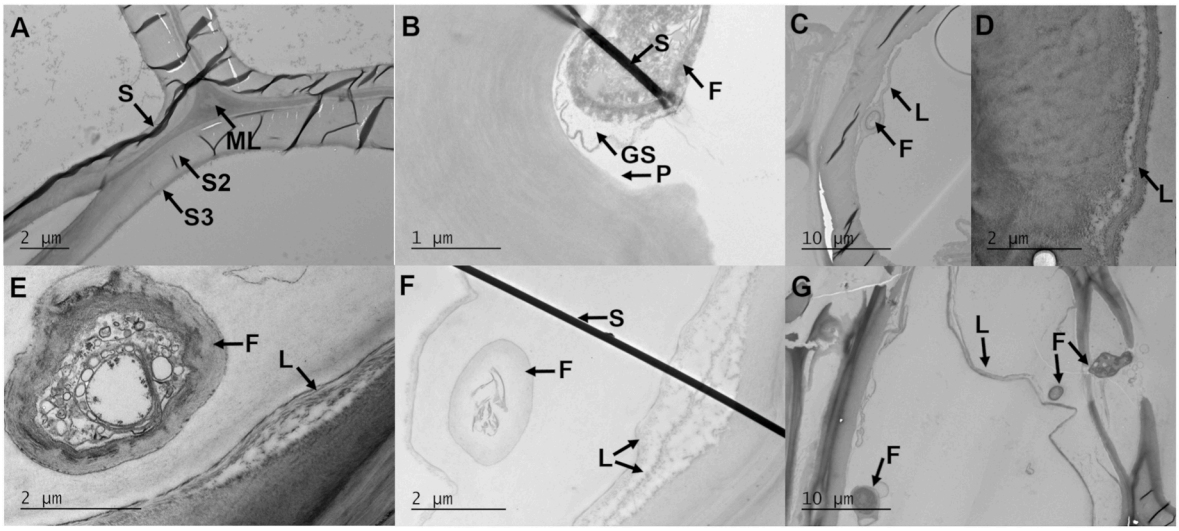

Fig. 7. TEM images of cross sections of spruce veneer slices after 1 y of fungal growth. (A) Non-inoculated wood; (B) *F. pinicola* inhabited, brown rot decayed wood; (C–D) *T. abietinum* colonized and degraded wood; (E–F) *P. radiata* colonized, white rot decayed wood; (G) spruce wood colonized with the brown rot and white rot fungal pair FpPr. S = dark stretch of polymeric embedding material, ML = middle lamellae, S2 = secondary cell wall layer 2, S3 = secondary cell wall layer 3, F = cross section of fungal hypha, GS = glucan sheath at the hyphal tip, P = signs of degradation of the wood secondary cell wall near the hyphal tip and glucan sheath, L = detaching wood cell wall layers. Scale bars are 2 μm (A, D-F), 1 μm (B), and 10 μm (C, G).

interspecific mycelial contact on Pr-produced manganese-peroxidase activity levels and on Fp-produced iron-reduction activity values was obvious (Fig. 5). Both activities were high at a short distance from the hyphal contact interaction zone towards the Pr and Fp mycelium sides, respectively. Decreasing gradients of MnP and iron reduction activities were detected on opposite sides of the interaction zone. Together with iron-reduction values, concentration of wood-bound oxalate was 1.65-fold higher on the brown rot Fp mycelium side (Fig. 5), showing a decreasing gradient towards the Fp-Pr interspecific interaction zone. On the Pr mycelium side, oxalate was not detected (under analytical detection limit).

In contrast, laccase activity was at the highest level in the contact zone and somewhat lower (60–80% of the interaction zone activity) at a short distance from the contact zone (Fig. 5). Interestingly, laccase activity was also observed on the brown rot Fp mycelium side, although almost no laccase activity was produced on the Fp single-species veneer cultivations (Fig. 4A).

3.4. Wood mass loss and Klason lignin content

Within 12 months, the dry weight of spruce wood veneer slices decreased (as mass loss) 37% in the brown rot Fp single-species cultivations (Table 3). With the white rot fungi alone (Pr or Ta), the wood mass loss was significantly lower, approximately ½ of the mass loss obtained with Fp. In the case of PrTa white rot-white rot species combination, wood mass loss was, however, somewhat greater than in the single-species cases. With other fungal combinations, FpPr pair was more similar to the Fp single-species case than the other pair FpTa or the combination of three fungi (FpPrTa).

In contrast to wood mass loss, the Klason lignin content relatively increased in the spruce wood veneers cultivated with the brown rot fungus Fp alone (32% lignin content in wood) and a little with the white rot fungus Pr alone (23% lignin content in wood), in comparison to the control spruce veneer slices incubated one year without fungi (21% lignin content in wood; Table 4). Although the relative Klason lignin content of the decayed spruce wood increased, the calculated total lignin loss was approximately 15% in the case of the white rot fungus Pr when taking into account the wood-mass loss during the twelve months. In the FpPr brown rot-white rot combination, the Klason lignin content in the interaction zone was as high as 47% (Table 4). These increments were statistically significant ($p < 0.05$). Acid-soluble lignin values increased in the single-species (Fp or Pr) and in the brown rot-white rot FpPr combination.

3.5. SEM and TEM of decayed spruce wood ultrastructure

Wood ultrastructure SEM images indicated that after 12 months of brown rot decay by Fp, the spruce xylem tracheid walls became more porous and loose compared to the structure of non-inoculated wood (Fig. 6A–C). In the wood decayed by Fp, crystalline deposits were visible as attached to the surfaces of decomposed wood cell walls in between the thin threads of fungal hyphae (Fig. 6B). After twelve months of white rot decay by Pr or Ta, wood tracheid cell walls became very thin and eroded, showing the cell wall layers as detaching (“peeling”) from each other (Fig. 6D–F).

Visible differences in the spruce wood ultrastructure between brown rot and white rot decay were apparent in the TEM images (Fig. 7). Hyphal tips of the brown rot fungus Fp exhibited excavation and intrusion into the spruce tracheid cell wall and coverage of the hyphal tip by extracellular matrix (glucan sheath, see Discussion) (Fig. 7B). However, the white rot fungi Pr and Ta exhibited a very different strategy of wood cell-wall degradation. After one year of white rot decay, the spruce tracheid wall compactness was lost and the remnants of the substantially thinned secondary cell-wall layers were loose and detached “layer by layer” (Fig. 7F). In both brown rot (Fp) and white rot (Pr or Ta) fungal occupation of the spruce xylem, the hyphae attached close to the S3 layer in the tracheid lumen space (Fig. 7C, E-G). With the white rot fungi Pr and Ta, hyphae were occasionally localized between the degraded, loosened cell-wall layers next to an intact cell wall (Fig. 7 C, F and G). Spruce tracheid bordered pits were one route for the fungal hyphae to enter the lumen of the next tracheid (Fig. 7 G).

4. Discussion

In this study, we observed that after 1 y of decomposition of spruce wood the presence of interspecifically interacting hyphae affected fungal enzymatic and metabolic activities, such as the lignin-attacking oxidoreductases (manganese peroxidase, lignin peroxidase and laccase) and brown-rot indicative iron reduction activity. Activity responses were observed at transcript level as differences in expression of specific white rot Pr (*P. radiata*) and brown rot Fp (*F. pinicola*) enzyme-encoding genes during mycelial interactions. Our results indicate that the white-rot decay signifying peroxidases as well as brown-rot signifying Fe^{2+}-dependent radical chemistry were partially repressed or inhibited due to the interspecific mycelial contacts. In contrast to these responses, laccase activities produced by the white rot species were stimulated in the interacting fungal combinations.

The white rot fungi of *Basidiomycota* class *Agaricomycetes* possess multiple genes for lignin-attacking high-redox class-II peroxidases (Hofrichter et al. 2010; Floudas et al. 2012); these genes are absent from the genomes of *Agaricomycetes* brown rot fungi (Eastwood et al., 2011; Ruiz-Dueñas et al. 2013; Riley et al. 2014). Therefore, we concentrated on the *P. radiata* class-II peroxidase genes *mnp2* and *lip2* (Mäkinen et al. 2019) which previously exhibited upregulation when the fungus was growing on spruce wood and lignocellulose substrates (Kuuskeri et al. 2016; Mäkinen et al. 2018). After 12 months of growth on the spruce wood veneers, expression of the Pr oxidoreductase encoding genes *mnp2* and *lpmo1* were at high level in the presence of the brown rot fungus Fp. This indicates potential co-regulation of the genes encoding a specific Pr manganese peroxidase and a lytic polysaccharide monooxygenase. Fp had a positive effect on expression of Pr *lip2* gene, which implies to differential regulation of the ten class-II peroxidase (MnP and LiP) encoding genes in *P. radiata* (Hildén et al. 2005, 2006; Mäkinen et al. 2019).

It is known from previous studies that among the multigene family encoding MnP, VP and LiP peroxidases in white rot fungi, gene-specific regulation is observed under changing conditions of substrate and nutrients, atmosphere, and chemical agents (Cohen et al. 2002; Hildén et al. 2005; Vanden Wymelenberg et al. 2009; Mattila et al. 2020). In contrast to our results, no expression of LiP-encoding genes was observed in the interaction zone of the white rot fungus *Trametes versicolor* paired with four other wood decay fungi for a short cultivation time (two or eight days) (Hiscox et al. 2010). However, the authors observed expression of one LiP-encoding gene behind the hyphal interaction zone on the side of the *T. versicolor* mycelium. This may indicate induction of a specific *lip* gene in the fungus as a response to hyphal interaction, which is similar to our observation with *lip2* expression in *P. radiata*. Production of MnP activity in white rot fungi is influenced by the presence of other fungal mycelia in co-cultures and on wood substrate (Baldrian 2004; Chi et al. 2007; Hiscox et al. 2010). Our results furthermore indicate attenuation by the brown rot fungal mycelium on white rot MnP activity in the Fp-Pr interaction zones - either through direct inhibition of enzyme activity or indirectly by suppression of gene expression in the white rot mycelia.

After 1 y of interactive growth on spruce wood, increase in laccase activity was detectable in the mycelial zones of the white rot fungi Pr and Ta. Activity pattern in the Fp-Pr contact zone also indicated a positive effect of interspecies mycelial interaction on Pr laccase production, which was observed in all fungal combinations on the spruce veneers. Fungal mycelial interactions include sensing, communication and responding at close proximity or at a distance between the hyphae of the encountering species, which may result e.g., with production and secretion of enzymes (Aleklett and Boddy 2021). Induction of laccase activity has been detected during interspecific interactions of *Basidiomycota* in other studies as well (Baldrian 2004; Hiscox et al. 2010). Upregulation of oxidoreductase-encoding genes was observed in a recent study on wood substrate for the *Agaricomycetes* brown rot species *Rhodonia placenta* that encountered another brown rot species *Gloeophyllum trabeum* (Presley et al. 2020). In our study, the Fp laccase-like oxidoreductase-encoding gene *mco1* was expressed at high transcript levels in the brown rot - white rot Fp-Pr interaction zone of the three-species combination FpPrTa. Thus, it may be concluded that interspecies interactions lead to increased expression of laccase-like enzyme encoding genes in fungi, also in the brown rot species, irrespective of the wood decay type caused by the confronting fungal mycelium.

Our results of point to that Fp-generated iron reduction was suppressed and no more involved at the late stage of wood decay in the case of interaction with the white rot species Pr and Ta. Expression of the Fp *fr1* gene putatively coding a ferric reductase was suppressed in *F.*

pinicola by action of Pr in their mycelial interaction zone. Our previous study indicated that in combinations of brown rot and white rot fungi, spruce wood decomposition pattern was dominated by Fp brown rot during the earlier stages (1–3 months) of decay (Mali et al. 2019). In contrast to current results, in the previous experiments on spruce wood sawdust, no laccase or MnP activity were detected with Fp present in the fungal combinations, while iron reduction activity reached high levels (Mali et al. 2019). Fe^{3+} reduction capacity is recognized as an indication of ongoing Fenton chemistry producing strong ROS (e.g., HO• -) radicals (Arantes et al. 2009; Shah et al. 2013, 2018). These findings may indicate that when encountering a white rot fungal mycelium for a longer duration, the Fenton chemistry driven brown rot decay is suppressed, at least in the late stage of wood decay.

Total mass loss of the substrate spruce wood veneer slices after 1 y was 37% caused by the brown rot fungus Fp. In our previous study, the fungus exhibited over 20% mass loss of spruce wood sawdust already in three months under similar laboratory conditions (Mali et al. 2019). This indicates that the utilizable cellulose and hemicellulose components were consumed by Fp rapidly, within a few months, resulting in decelerated wood decomposition rate in the later phase of decay. The notably high Klason lignin content in the FpPr combination is another indication of efficient brown rot utilization of wood celluloses and hemicelluloses by Fp, leading to increase in the relative proportion of lignin in the decaying wood. Elevation in relative amount of lignin may restrict the attainability of available consumable cellulose and hemicellulose components, leading to a deceleration in the brown rot wood decay rate. Accumulation of acid-soluble lignin indicates that, however, both fungal brown rot and white rot degradative activities resulted in solubilization of aromatic (lignin-derived) compounds from spruce wood. In addition, decomposition of the spruce wood veneer slices, analysed as mass loss and proportions of Klason type and acid-soluble lignin were affected by the fungal species combination.

These data are consistent with previous results on the white rot fungus *P. radiata* demonstrating its ability to degrade wood lignin and even mineralize synthetic lignin (Moilanen et al. 1996; Hatakka et al. 2002; Niemenmaa et al. 2006; Kuuskeri et al. 2016). Lignin loss relative to density loss may be a promising method to distinguish wood decay types, from fungal white rot to brown rot and including intermediate and "grey rot" decay types. However, in fungal communities the wood decay type of an individual fungal species cannot be distinguished with this method. Instead, the proposed relation may be used to pinpoint development of the dominant rot type in mycelial interaction situations, and in decaying deadwood at the forest site.

Changes in spruce wood ultrastructure within 1 y of fungal growth were distinguished between brown rot decay produced by Fp and white rot decay generated by Pr or Ta, using SEM and TEM imaging. Deadwood inhabiting, wood-decaying filamentous fungi of *Basidiomycota* colonize their substrate by hyphal extension through the hollow lumen of the tracheids, thereby encountering the innermost secondary cell wall first (Daniel 1994). Previously, thinning of the spruce wood secondary cell walls by action of Pr was observed to occur in six weeks of hyphal colonization (Kuuskeri et al. 2016). This associated with attack and degradation of wood lignin. After one year, severe weakening of the spruce tracheid cell walls made by Pr was evident in our study. At this stage, consumption of cellulose microfibrils within the secondary cell walls obviously lead to wood softening and collapse of the tracheids due to simultaneous decay. However, brown rot decay by Fp weakened the spruce tracheids differentially; the wood cell walls became porous instead of thinning. Regions of brown rot and white rot were even distinctly visible in the respective mycelial zones of the interacting species combinations on the spruce veneer slices.

These distinct observations of fungal decomposition effects in wood ultrastructure are consistent with previous findings on the decay mechanisms of *P. radiata* and *F. pinicola*, and the *Agaricomycetes* white rot species *Pleurotus ostreatus* and brown rot species *G. trabeum* (Messner and Stachelberger 1984; Daniel 1994; Goodell et al. 2017; Bari et al. 2020). The whitish 0.5–1.0 μm wide particles observed in the SEM images of Fp are most likely calcium and other cation oxalate deposits attached onto decaying wood cell walls, as has been observed in previous studies (Dutton et al. 1993).

One specific feature of brown rot fungi is their strong production of oxalic acid during mycelial growth and decomposition of lignocellulose substrates (Takao 1965; Mäkelä et al. 2002; Niemenmaa et al. 2006; Arantes et al. 2012; Mali et al. 2017; Shah et al. 2018). Oxalic acid accumulates to high concentrations in cultures of *F. pinicola* (Mali et al., 2019; Shah et al., 2018). Large proportion of fungal secreted oxalic acid may dissociate and become either attached to the substrate wood cell walls as oxalate ions (Mali et al. 2019) or chelated with cations into solid deposits. In this study, some wood-bound oxalate was found in the brown rot Fp-decomposed spruce wood, and crystalline deposits were seen in the SEM images, whereas only minor quantities were detectable while Fp was interacting with the white rot fungus Pr. Furthermore, no oxalate was detected on the Pr mycelium side of the Fp- Pr hyphal interaction zone. These findings point to an ability of Pr to eliminate excess extracellular oxalic acid in its growth environment. In white rot fungi, genes encoding the oxalic-acid degrading enzyme oxalate decarboxylase are identified (Mäkelä et al. 2010; Mäkinen et al. 2019). Thus, degradation of oxalic acid can be an additional defence mechanism of white rot fungi in mycelial contacts with brown rot fungi to eliminate success of the encountering species and its decay mechanism, thereby conquering in fungal competition.

Our TEM images indicate that the hyphae of the brown rot fungus *F. pinicola* form a shielding extracellular matrix. The matrix is most likely composed of fungal-secreted extracellular and branched glucan polysaccharides (Ruel and Joseleau 1991). The glucan matrix may act as protective gel for the elongating hyphal tip, as well as a water-containing matrix immobilizing secreted enzymes, peptides, and secondary and primary metabolites such as oxalate (Eriksson et al. 1990; Ruel and Joseleau 1991; Dutton et al. 1993; Daniel 1994; Arantes et al. 2012). In addition, our findings support the theory of a "staggered mechanism" of brown rot decay generated by the extending hyphae in wood (Zhang et al. 2016; Presley and Schilling, 2017).

5. Conclusion

Mycelial interspecific interactions in varying combinations affected expression of genes encoding signature wood-decay enzymes, suppressed brown rot activity, influenced activities and production of enzymes such as laccase and manganese peroxidase, and changed the pattern of late-stage decay of wood from brown rot to white rot decomposition mechanism. Altogether, it seems that the mycelial encounter-interaction zones are specific not only to the fungal species combination but also to the phase and dominating type of wood decomposition. Our results indicate a transition from extensive brown rot to a late-stage white rot along advancement of wood decomposition. This is apparently due to processive fungal hyphal growth and metabolism causing changes in the overall biochemical and structural composition of the decaying wood substrate.

Funding

This work was supported by Jane and Aatos Erkko foundation [grant number 170101 to T.L.] and the Microbiology and Biotechnology Doctoral Program, University of Helsinki, doctoral study position to T. M.

Declaration of competing interest

All authors declare that they have no conflicts of interest.

Acknowledgements

We thank Mari A. Mäkinen and Hans K. Mattila for their assistance and experience in real-time qRT-PCR and HPLC analyses, respectfully. We thank the EMBI Electron Microscopy Unit (https://www.helsinki.fi/en/infrastructures/bioimaging/embi) of the Helsinki Institute of Life Science, University of Helsinki, for their excellent services and use of the infrastructure.

References

Aleklett, K., Boddy, L., 2021. Fungal behaviour: a new frontier in behavioural ecology. Trends Ecol. Evol. 36 (9), 787–796. https://doi.org/10.1016/j.tree.2021.05.006.

Arantes, V., Jellison, J., Goodell, B., 2012. Peculiarities of brown-rot fungi and biochemical Fenton reaction with regard to their potential as a model for bioprocessing biomass. Appl. Microbiol. Biotechnol. 94 (2), 323–338. https://doi.org/10.1007/s00253-012-3954-y.

Arantes, V., Qian, Y., Milagres, A.M.F., Jellison, J., Goodell, B., 2009. Effect of pH and oxalic acid on the reduction of Fe^{3+} by a biomimetic chelator and on Fe^{3+} desorption/adsorption onto wood: implications for brown-rot decay. Int. Biodeterior. Biodegrad. 63 (4), 478–483. https://doi.org/10.1016/j.ibiod.2009.01.004.

Baldrian, P., 2004. Increase of laccase activity during interspecific interactions of white-rot fungi. FEMS (Fed. Eur. Microbiol. Soc.) Microbiol. Ecol. 50 (3), 245–253. https://doi.org/10.1016/j.femsec.2004.07.005.

Baldrian, P., 2017. Forest microbiome: diversity, complexity and dynamics. FEMS (Fed. Eur. Microbiol. Soc.) Microbiol. Rev. 41 (2), 109–130. https://doi.org/10.1093/femsre/fuw040.

Bari, E., Daniel, G., Yilgor, N., Kim, J.S., Tajick-Ghanbary, M.A., Singh, A.P., Ribera, J., 2020. Comparison of the decay behavior of two white-rot fungi in relation to wood type and exposure conditions. Microorganisms 8, 1931. https://doi.org/10.3390/microorganisms8121931.

Browning, B.L., 1967. Methods of Wood Chemistry. Interscience Publishers, New York, p. 882.

Castanera, R., López-Varas, L., Pisabarro, A.G., Ramírez, L., 2015. Validation of reference genes for transcriptional analyses in *Pleurotus ostreatus* by using reverse transcription-quantitative PCR. Appl. Environ. Microbiol. 81, 4120–4129. https://doi.org/10.1128/AEM.00402-15.

Chi, Y., Hatakka, A., Maijala, P., 2007. Can co-culturing of two white-rot fungi increase lignin degradation and the production of lignin-degrading enzymes? Int. Biodeterior. Biodegrad. 59 (1), 32–39. https://doi.org/10.1016/j.ibiod.2006.06.025.

Cohen, R., Yarden, O., Hadar, J., 2002. Lignocellulose affects $Mn2^{+}$ regulation of peroxidase transcript levels in solid-state cultures of *Pleurotus ostreatus*. Appl. Environ. Microbiol. 68 (6), 3156–3158. https://doi.org/10.1128/aem.68.6.3156-3158.2002.

Daniel, G., 1994. Use of electron microscopy for aiding our understanding of wood biodegradation. FEMS (Fed. Eur. Microbiol. Soc.) Microbiol. Rev. 13, 199–233. https://doi.org/10.1111/j.1574-6976.1994.tb00043.x.

Dutton, M.V., Evans, C.S., Atkey, P.T., Wood, D.A., 1993. Oxalate production by Basidiomycetes, including the white-rot species *Coriolus versicolor* and *Phanerochaete chrysosporium*. Appl. Microbiol. Biotechnol. 39, 5–10. https://doi.org/10.1007/BF00166839.

Eastwood, D.C., Floudas, D., Binder, M., Majcherczyk, A., Schneider, P., Aerts, A., Asiegbu, F.O., Baker, S.E., Barry, K., Bendiksby, M., Blumentritt, M., Coutinho, P.M., Cullen, D., de Vries, R.P., Gathman, A., Goodell, B., Henrissat, B., Ihrmark, K., Kauserud, H., Kohler, A., LaButti, K., Lapidus, A., Lavin, J.L., Lee, Y.H., Lindquist, E., Lilly, W., Lucas, S., Morin, E., Murat, C., Oguiza, J.A., Park, J., Pisabarro, A.G., Riley, R., Rosling, A., Salamov, A., Schmidt, O., Schmutz, J., Skrede, I., Stenlid, J., Wiebenga, A., Xie, X., Kües, U., Hibbett, D.S., Hoffmeister, D., Högberg, N., Martin, F., Grigoriev, I.V., Watkinson, S.C., 2011. The plant cell wall-decomposing machinery underlies the functional diversity of forest fungi. Science 333 (6043), 762–765. https://doi.org/10.1126/science.1205411.

El Ariebi, N., Hiscox, J., Scriven, S.A., Müller, C.T., Boddy, L., 2016. Production and effects of volatile organic compounds during interspecific interactions. Fungal Ecol. 20, 144–154. https://doi.org/10.1016/j.funeco.2015.12.013.

Eriksson, K.-E.L., Blanchette, R.A., Ander, P., 1990. Microbial and enzymatic degradation of wood and wood components. In: Springer Series in Wood Science. Springer, Berlin, Heidelberg, p. 407.

Floudas, D., Binder, M., Riley, R., Barry, K., Blanchette, R.A., Henrissat, B., Martínez, A. T., Otillar, R., Spatafora, J.W., Yadav, J.S., Aerts, A., Benoit, I., Boyd, A., Carlson, A., Copeland, A., Coutinho, P.M., de Vries, R.P., Ferreira, P., Findley, K., Foster, B., Gaskell, J., Glotzer, D., Górecki, P., Heitman, J., Hesse, C., Hori, C., Igarashi, K., Jurgens, J.A., Kallen, N., Kersten, P., Kohler, A., Kües, U., Kumar, T.K., Kuo, A., LaButti, K., Larrondo, L.F., Lindquist, E., Ling, A., Lombard, V., Lucas, S., Lundell, T., Martin, R., McLaughlin, D.J., Morgenstern, I., Morin, E., Murat, C., Nagy, L.G., Nolan, M., Ohm, R.A., Patyshakuliyeva, A., Rokas, A., Ruiz-Dueñas, F.J., Sabat, G., Salamov, A., Samejima, M., Schmutz, J., Slot, J.C., St John, F., Stenlid, J., Sun, H., Sun, S., Syed, K., Tsang, A., Wiebenga, A., Young, D., Pisabarro, A., Eastwood, D.C., Martin, F., Cullen, D., Grigoriev, I.V., Hibbett, D.S., 2012. The Paleozoic origin of enzymatic lignin decomposition reconstructed from 31 fungal genomes. Science 336 (6089), 1715–1719. https://doi.org/10.1126/science.1221748.

Goodell, B., Zhu, Y., Kim, S., Kafle, K., Eastwood, D., Daniel, G., Jellison, J., Yoshida, M., Groom, L., Pingali, S.V., O'Neill, H., 2017. Modification of the nanostructure of lignocellulose cell walls via a non-enzymatic lignocellulose deconstruction system in brown rot wood-decay fungi. Biotechnol. Biofuels 10, 179. https://doi.org/10.1186/s13068-017-0865-2.

Hatakka, A., Maijala, P., Mettälä, A., Hakala, T., Hauhio, L., Ellmén, J., 2002. Fungi as potential assisting agents in softwood pulping. Prog. Biotechnol. 21, 81–88. https://doi.org/10.1016/S0921-0423(02)80010-7.

Hatfield, R., Fukushima, R.S., 2004. Can lignin be accurately measured? Crop Sci. 45, 832–839. https://doi.org/10.2135/cropsci2004.0238.

Hildén, K., Mäkelä, M.R., Hakala, T.K., Hatakka, A., Lundell, T., 2006. Expression on wood, molecular cloning and characterization of three lignin peroxidase (LiP) encoding genes of the white rot fungus *Phlebia radiata*. Curr. Genet. 49, 97–105. https://doi.org/10.1007/s00294-005-0045-y.

Hildén, K., Martinez, A.T., Hatakka, A., Lundell, T., 2005. The two manganese peroxidases Pr-MnP2 and Pr-MnP3 of *Phlebia radiata*, a lignin degrading basidiomycete, are phylogenetically and structurally divergent. Fungal Genet. Biol. 42, 403–419. https://doi.org/10.1016/j.fgb.2005.01.008.

Hiscox, J., Baldrian, P., Rogers, H.J., Boddy, L., 2010. Changes in oxidative enzyme activity during interspecific mycelial interactions involving the white-rot fungus *Trametes versicolor*. Fungal Genet. Biol. 47, 562–571. https://doi.org/10.1016/j.fgb.2010.03.007.

Hofrichter, M., Ullrich, R., Pecyna, M.J., Liers, C., Lundell, T., 2010. New and classic families of secreted fungal heme peroxidases. Appl. Microbiol. Biotechnol. 87, 871–897. https://doi.org/10.1007/s00253-010-2633-0.

Kuuskeri, J., Häkkinen, M., Laine, P., Smolander, O.-P., Tamene, F., Miettinen, S., Nousiainen, P., Kemell, M., Auvinen, P., Lundell, T., 2016. Time-scale dynamics of proteome and transcriptome of the white-rot fungus *Phlebia radiata*: growth on spruce wood and decay effect on lignocellulose. Biotechnol. Biofuels 9, 192. https://doi.org/10.1186/s13068-016-0608-9.

Kuuskeri, J., Mäkelä, M.R., Isotalo, J., Oksanen, I., Lundell, T., 2015. Lignocellulose-converting enzyme activity profiles correlate with molecular systematics and phylogeny grouping in the incoherent genus *Phlebia* (Polyporales, Basidiomycota). BMC Microbiol. 15, 217. https://doi.org/10.1186/s12866-015-0538-x.

Llanos, A., François, J., Parrou, J.-L., 2015. Tracking the best reference genes for RT-qPCR data normalization in filamentous fungi. BMC Genom. 16, 71. https://doi.org/10.1186/s12864-015-1224-y.

Lombard, V., Golaconda, R., Drula, E., Coutinho, P.M., Henrissat, B., 2014. The Carbohydrate-active enzymes database (CAZy) in 2013. Nucleic Acids Res. 42 (D1), D490–D495. https://doi.org/10.1093/nar/gkt1178.

Lundell, T.K., Mäkelä, M.R., de Vries, R.P., Hildén, K.S., 2014. Genomics, lifestyles and future prospects of wood decay and litter-decomposing Basidiomycota. Adv. Bot. Res. 70, 329–370. https://doi.org/10.1016/B978-0-12-397940-7.00011-2.

Mäkelä, M., Galkin, S., Hatakka, A., Lundell, T., 2002. Production of organic acids and oxalate decarboxylase in lignin-degrading white rot fungi. Enzym. Microb. Technol. 30 (4), 542–549. https://doi.org/10.1016/S0141-0229(02)00012-1.

Mäkelä, M.R., Hilden, K., Lundell, T.K., 2010. Oxalate decarboxylase: biotechnological update and prevalence of the enzyme in filamentous fungi. Appl. Microbiol. Biotechnol. 87 (3), 801–814. https://doi.org/10.1007/s00253-010-2650-z.

Mäkinen, M., Kuuskeri, J., Laine, P., Smolander, O.-P., Kovalchuk, A., Zeng, Z., Asiegbu, F., Paulin, L., Auvinen, P., Lundell, T., 2019. Genome description of *Phlebia radiata* 79 with comparative genomics analysis on lignocellulose decomposition machinery of phlebioid fungi. BMC Genom. 20, 430. https://doi.org/10.1186/s12864-019-5817-8.

Mäkinen, M., Risulainen, N., Mattila, H., Lundell, T.K., 2018. Transcription of lignocellulose-decomposition associated genes, enzyme activities and production of ethanol upon bioconversion of waste substrate by *Phlebia radiata*. Appl. Microbiol. Biotechnol. 102, 5657–5672. https://doi.org/10.1007/s00253-018-9045-y.

Mali, T., Kuuskeri, J., Shah, F., Lundell, T.K., 2017. Interactions affect hyphal growth and enzyme profiles in combinations of coniferous wood-decaying fungi of Agaricomycetes. PLoS One 12 (9), e0185171. https://doi.org/10.1371/journal.pone.0185171.

Mali, T., Mäki, M., Hellén, H., Heinonsalo, J., Bäck, J., Lundell, T., 2019. Decomposition of spruce wood and release of volatile organic compounds depend on decay type, fungal interactions and enzyme production patterns. FEMS (Fed. Eur. Microbiol. Soc.) Microbiol. Ecol. 95 https://doi.org/10.1093/femsec/fiz135 fiz135.

Mattila, H., Kuuskeri, J., Lundell, T., 2017. Single-step, single-organism bioethanol production and bioconversion of lignocellulose waste materials by phlebioid fungal species. Bioresour. Technol. 225, 254–261.

Mattila, H.K., Mäkinen, M., Lundell, T., 2020. Hypoxia is regulating enzymatic wood decomposition and intracellular carbohydrate metabolism in filamentous white rot fungus. Biotechnol. Biofuels 13, 26. https://doi.org/10.1186/s13068-020-01677-0.

Messner, K., Stachelberger, H., 1984. Transmission electron microscopy observations of brown rot caused by *Fomitopsis pinicola* with respect to osmiophilic particles. Trans. Br. Mycol. Soc. 83 (1), 113–130. https://doi.org/10.1016/S0007-1536(84)80251-X.

Moilanen, A., Lundell, T., Vares, T., Hatakka, A., 1996. Manganese and malonate are individual regulators for the production of lignin and manganese peroxidase isozymes and in the degradation of lignin by *Phlebia radiata*. Appl. Microbiol. Biotechnol. 45 (6), 792–799. https://doi.org/10.1007/s002530050764.

Nagy, L.G., Riley, R., Tritt, A., Adam, C., Daum, C., Floudas, D., Sun, H., Yadav, J.S., Pangilinan, J., Larsson, K.H., Matsuura, K., Barry, K., Labutti, K., Kuo, R., Ohm, R.A., Bhattacharya, S.S., Shirouzu, T., Yoshinaga, Y., Martin, F.M., Grigoriev, I.V., Hibbett, D.S., 2016. Comparative genomics of early-diverging mushroom-forming fungi provides insights into the origins of lignocellulose decay capabilities. Mol. Biol. Evol. 33 (4), 959–970. https://doi.org/10.1093/molbev/msv337.

Niemenmaa, O., Uusi-Rauva, A., Hatakka, A., 2006. Wood stimulates the demethoxylation of [$O^{14}CH_3$]-labelled lignin model compounds by the white-rot

fungi *Phanerochaete chrysosporium* and *Phlebia radiata*. Arch. Microbiol. 185 (4), 307–315. https://doi.org/10.1007/s00203-006-0097-5.

Ottosson, E., Nordén, J., Dahlberg, A., Edman, M., Jönsson, M., Larsson, K.-H., Olsson, J., Penttilä, R., Stenlid, J., Ovaskainen, O., 2014. Species associations during the succession of wood-inhabiting fungal communities. Fungal Ecol. 11, 17–28. https://doi.org/10.1016/j.funeco.2014.03.003.

Ovaskainen, O., Schigel, D., Ali-Kovero, H., Auvinen, P., Paulin, L., Nordén, B., Nordén, J., 2013. Combining high-throughput sequencing with fruit body surveys reveals contrasting life-history strategies in fungi. ISME J. 7, 1696–1709. https://doi.org/10.1038/ismej.2013.61.

Presley, G.N., Schilling, J.S., 2017. Distinct growth and secretome strategies by two taxonomically divergent brown rot fungi. Appl. Environ. Microbiol. 83, e02987-16 https://doi.org/10.1128/AEM.02987-16.

Presley, G.N., Zhang, J., Purvine, S.O., Schilling, J.S., 2020. Functional genomics, transcriptomics, and proteomics reveal distinct combat strategies between lineages of wood-degrading fungi with redundant wood decay mechanisms. Front. Microbiol. 11, 1646. https://doi.org/10.3389/fmicb.2020.01646.

Rajala, T., Peltoniemi, M., Hantula, J., Mäkipää, R., Pennanen, T., 2011. RNA reveals a succession of active fungi during the decay of Norway spruce logs. Fungal Ecol. 4, 437–448. https://doi.org/10.1016/j.funeco.2011.05.005.

Rajala, T., Tuomivirta, T., Pennanen, T., Mäkipää, R., 2015. Habitat models of wood-inhabiting fungi along a decay gradient of Norway spruce logs. Fungal Ecol. 18, 48–55. https://doi.org/10.1016/j.funeco.2015.08.007.

Riley, R., Salamov, A.A., Brown, D.W., Nagy, L.G., Floudas, D., Held, B.W., Levasseur, A., Lombard, V., Morin, E., Otillar, R., Lindquist, E.A., Sun, H., LaButti, K.M., Schmutz, J., Jabbour, D., Luo, H., Baker, S.E., Pisabarro, A.G., Walton, J.D., Blanchette, R.A., Henrissat, B., Martin, F., Cullen, D., Hibbett, D.S., Grigoriev, I.V., 2014. Extensive sampling of basidiomycete genomes demonstrates inadequacy of the white-rot/brown-rot paradigm for wood decay fungi. PNA 111 (27), 9923–9928. https://doi.org/10.1073/pnas.1400592111.

Ruel, K., Joseleau, J.-P., 1991. Involvement of an extracellular glucan sheat during degradation of Populus wood by *Phanerochaete chrysosporium*. Appl. Environ. Microbiol. 57 (2), 374–384. https://doi.org/10.1128/aem.57.2.374-384.1991.

Ruiz-Dueñas, FJ, Lundell, T, Floudas, D, Nagy, LG, Barrasa, JM, Hibbett, DS, Martinez, AT, 2013. Lignin-degrading peroxidases in Polyporales: an evolutionary survey based on 10 sequenced genomes. Mycologia 105, 1428–1444. https://doi.org/10.3852/13-059.

Rytioja, J., Hildén, K., Hatakka, A., Mäkelä, M.R., 2014. Transcriptional analysis of selected cellulose-acting enzymes encoding genes of the white-rot fungus *Dichomitus squalens* on spruce wood and microcrystalline cellulose. Fungal Genet. Biol. 72, 91–98.

Shah, F., Mali, T., Lundell, T.K., 2018. Polyporales brown rot species *Fomitopsis pinicola*: enzyme activity profiles, oxalic acid production, and Fe^{3+}-reducing metabolite secretion. Appl. Environ. Microbiol. 84 (8), e02662-17 https://doi.org/10.1128/AEM.02662-17.

Shah, F., Rineau, F., Canbäck, B., Johansson, T., Tunlid, A., 2013. The molecular components of the extracellular protein-degradation pathways of the ectomycorrhizal fungus *Paxillus involutus*. New Phytol. 200 (3), 875–887. https://doi.org/10.1111/nph.12425.

Shah, F., Schwenk, D., Nicolas, C., Persson, P., Hoffmeister, D., Tunlid, A., 2015. Involutin is a Fe^{3+} reductant secreted by the ectomycorrhizal fungus *Paxillus involutus* during Fenton-based decomposition of organic matter. Appl. Environ. Microbiol. 81, 8427–8433, 10.1128%2FAEM.02312-15.

Steiger, M.G., Mach, R.L., Mach-Aigner, A.R., 2010. An accurate normalization strategy for RT-qPCR in *Hypocrea jecorina* (*Trichoderma reesei*). J. Biotechnol. 145, 30–37. https://doi.org/10.1016/j.jbiotec.2009.10.012.

Sjöström, E., 1993. Wood Chemistry: Fundamentals and Applications, second ed. Academic Press, San Diego, California, p. 293.

Slomczynski, D., Nakas, J.P., Tanenbaum, S.W., 1995. Production and characterization of laccase from Botrytis cinerea. Appl. Environ. Microbiol. 61, 907–912. https://doi.org/10.1128/aem.61.3.907-912.1995.

Takao, S., 1965. Organic acid production by Basidiomycetes. I. Screening of acid-producing strains. Appl. Microbiol. 13 (5), 732–737. https://doi.org/10.1128/am.13.5.732-737.1965.

Vanden Wymelenberg, A., Gaskell, J., Mozuch, M., Kersten, P., Sabat, G., Martinez, D., Cullen, D., 2009. Transcriptome and secretome analyses of *Phanerochaete chrysosporium* reveal complex patterns of gene expression. Appl. Environ. Microbiol. 75, 4058–4068. https://doi.org/10.1128/aem.00314-09.

Wariishi, H., Valli, K., Gold, M.H., 1992. Manganese(II) oxidation by manganese peroxidase from the basidiomycete Phanerochaete chrysosporium. Kinetic mechanism and role of chelators. J. Biol. Chem. 267, 23688–23695. https://doi.org/10.1016/S0021-9258(18)35893-9.

Warton, D.I., Hui, F.K.C., 2011. The arcsine is asinine: the analysis of proportions in ecology. Ecology 92, 3–10.

Xu, G., Goodell, B., 2001. Mechanisms of wood degradation by brown-rot fungi: chelator-mediated cellulose degradation and binding of iron by cellulose. J. Biotechnol. 87, 43–57. https://doi.org/10.1016/S0168-1656(00)00430-2.

Yakovlev, I.A., Hietala, A.M., Courty, P.-E., Lundell, T., Solheim, Fossdal, C.G., 2013. Genes associated with lignin degradation in the polyphagous white-rot pathogen *Heterobasidion irregulare* show substrate-specific regulation. Fungal Genet. Biol. 56, 17–24. https://doi.org/10.1016/j.fgb.2013.04.011.

Zhang, J., Presley, G.N., Hammel, K.E., Ryu, J.-S., Menke, J.R., Figueroa, M., Hu, D., Orr, G., Schilling, J.S., 2016. Localizing gene regulation reveals a staggered wood decay mechanism for the brown rot fungus *Postia placenta*. PNA 113, 10968–10973. https://doi.org/10.1073/pnas.1608454113.